Rayleigh scattering limits for low-level bidirectional reflectance distribution function measurements

C. Asmail, J. Hsia, A. Parr, and J. Hoeft

The objective is to estimate the Rayleigh limit in bidirectional reflectance distribution function (BRDF) measurements caused by air in the laboratory, the wavelength, and the path length of light in the receiver field of view. Moreover, we intend to show the trend for the reduction of this limit by introducing a medium with small refractive index and by using a longer wavelength. Although the BRDF typically describes the angular distribution of scattered light from surfaces, the expression describing the equivalent BRDF caused by the optical scattering from gas molecules in the optical path is derived through the use of the Rayleigh scattering theory. The instrumentation is described, and the experimental results of the equivalent BRDF caused by gas scattering from molecules in clear air, nitrogen, and helium gases are reported. These results confirm the trends of the prediction.

Key words: Bidirectional reflectance distribution function (BRDF), equivalent BRDF, instrument-signature measurements, instrumentation, optical scatter from surfaces, photon scattering, Rayleigh scattering, theoretical analysis of the equivalent BRDF, vertically polarized incident light.

1. Introduction

The bidirectional reflectance distribution function (BRDF) of a surface describes the angular distribution of scattered radiance reflected by a surface normalized by the incident irradiance on the surface.[1] System noise from BRDF instrumentation becomes significant when one measures specularly reflecting surfaces that exhibit very low scatter levels at angles that differ from the specular direction. The BRDF caused by instrument limitations when there is no sample scatterer present is called the equivalent BRDF. (The equivalent BRDF is also called the instrument signature.[2]) Typically, an equivalent BRDF measurement is carried out to show the lowest BRDF that an instrument can measure.

The equivalent BRDF[3,4] has many sources, including scatter from optical components located within the measuring system, internal reflections from mountings within the instrument, electronic noise, and scatter from the gas molecules contained within the field of view of the receiver system. This last factor is nonexistent for BRDF measurements made in a vacuum. Because most of the BRDF instruments are not contained within vacuum systems, an investigation of the effect on BRDF limits caused by this background scatter was conducted. For this purpose, a fixed-angle, low-electronic-noise BRDF system with two laser sources was designed, built, and tested with several gases present within the receiver's field of view. Here we present the theoretical derivation of the equivalent BRDF caused by the scattering of the gas molecules within the field of view of the receiver. We also describe the instrumentation and present the experimental results of the equivalent BRDF caused by scattering from gas molecules of clean air, nitrogen, and helium gases. These results are compared with the trends of the theoretical prediction.

2. Theoretical Analysis

We model the contribution to the equivalent BRDF from the gas molecules in the atmosphere contained within the field of view of the receiver by applying Rayleigh scattering theory.[5] In this section we derive the expression of the equivalent BRDF.

Figure 1 shows the configuration for the scattering problem. Appendix A gives the derivation for the irradiance at some point p caused by Rayleigh scatter-

J. Hoeft is with the Office of the Secretary of the U.S. Air Force, Washington, D.C. 22215; the other authors are with the Radiometric Physics Division, National Institute of Standards and Technology, Gaithersburg, Maryland 20899.

Received 19 April 1993; revised manuscript received 18 March 1994.

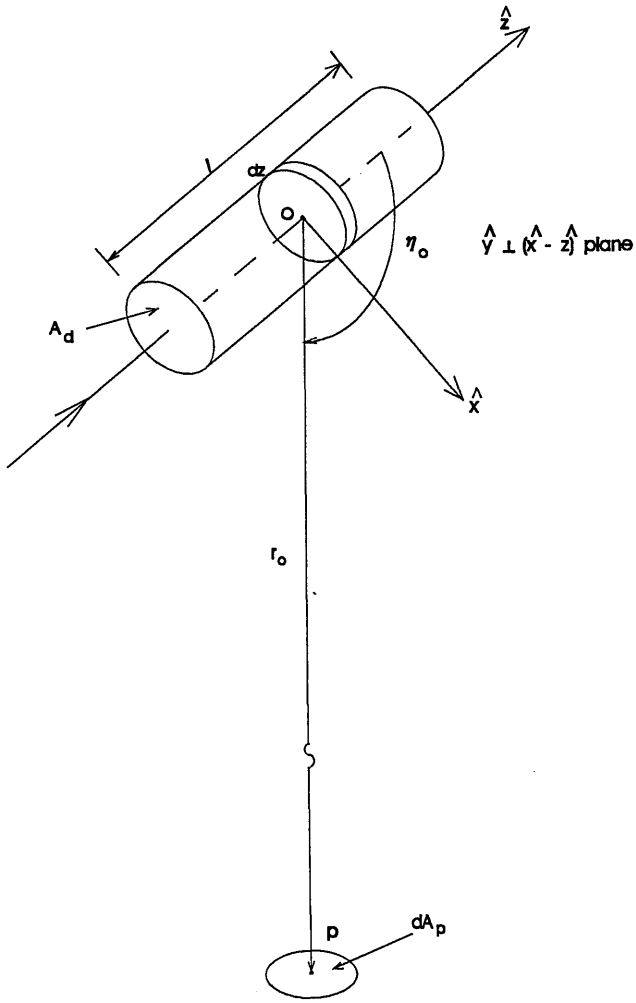

Fig. 1. Coordinates for scattering.

ing of vertically polarized light. A linearly polarized, collimated light beam with its electric vector in the y direction is propagating in the z direction. The light beam has a cross section of A_d with a path length of ℓ within the field of view of the receiver, which is positioned at point p in the x–z plane. The irradiance of the light beam at cross section A_d is E_i. The irradiance at p, E_p, caused by the scattering of vertically polarized light by one gas molecule can be expressed as [refer to Appendix A for the derivation of Eq. (1)]

$$E_p = \frac{k^4|\alpha|^2}{r_o^2} E_i, \tag{1}$$

where

k is the wave number, i.e., $2\pi/\lambda$,
λ is the wavelength of light used,
α is the polarizability with a dimension of $[m^3]$, i.e., $(3/4\pi N)(n^2 - 1/n^2 + 2)$,
N is the number of gas molecules per unit volume,
n is the index of refraction of the gas, and
r_o is the distance between the receiver at p and point O.

The number of gas molecules contained in a section of volume $A_d dz$ is $A_d dz N$. For a cross section A_d with a radius much smaller than r_o, the irradiance at p caused by the scattering of all the gas molecules in volume $A_d \ell$ can be written as

$$E_p' = \int_{-\ell/2}^{\ell/2} A_d N \frac{k^4|\alpha|^2}{r^2} E_i dz, \tag{2}$$

where

$$r^2 = r_o^2 + z^2 - 2 r_o z \cos \eta_0,$$

and where

r is the distance between p and any location along z within ℓ, and
η_o is the angle between the directions of the incident light beam and the receiver.

For a setup where ℓ is very small compared with r_o, $r^2 \cong r_o^2$, Eq. (2) can be simplified to

$$E_p' = \ell A_d N \frac{k^4|\alpha|^2}{r_o^2} E_i. \tag{3}$$

Next, the scattered radiance, L_s, from the gas molecules in volume $A_d \ell$, is expressed in terms of the irradiance at p, E_p'. The scattered flux from A_d collected at p is

$$\Phi_s = L_s d\omega_p |\cos \eta_o| A_d, \tag{4}$$

where $d\omega_p$ is the solid angle of the receiver subtended at p,

$$d\omega_p = A_p / r_o^2, \tag{5}$$

and A_p is the area of the receiver aperture stop. The scattered irradiance at p can be expressed radiometrically as

$$E_p' = \Phi_s / A_p. \tag{6}$$

Inserting Eqs. (5) and (6) into Eq. (4) and rearranging yield

$$L_s = \frac{E_p' r_o^2}{A_d - |\cos \eta_o|}. \tag{7}$$

Substituting E_p' from Eq. (3) yields

$$L_s = \ell N k^4 |\alpha|^2 E_i / |\cos \eta_o|. \tag{8}$$

The expression for the equivalent BRDF, f, caused by the scattering of the gas molecules in volume $A_d \ell$ is therefore given by

$$f \equiv \frac{L_s}{E_i}$$

$$f = \ell N k^4 |\alpha|^2 / |\cos \eta_o|. \tag{9}$$

Inserting the expressions for k and α gives

$$f = \ell N\left(\frac{2\pi}{\lambda}\right)^4\left(\frac{3}{4\pi N}\frac{n^2-1}{n^2+2}\right)^2\Big/|\cos\eta_o|,$$

$$= \ell N\left(\frac{2\pi}{\lambda}\right)^4\left(\frac{3}{4\pi N}\frac{(n-1)(n+1)}{(n^2+2)}\right)^2\Big/|\cos\eta_o|. \quad (10)$$

For n close to unity, $n^2 + 2 \approx 3$ and $n + 1 \approx 2$:

$$f = \frac{4\pi^2\ell}{\lambda^4 N}(n-1)^2/|\cos\eta_o|; \quad (11)$$

for the case of $\eta_o = 135°$,

$$f = 4\sqrt{2}\,\frac{\pi^2\ell(n-1)^2}{\lambda^4 N}. \quad (12)$$

Theoretically, this expression gives the lowest measurable equivalent BRDF at $\eta_o = 135°$ for vertically polarized incident light, a particular value of ℓ, and a given environment, if one assumes no other stray light. This quantity imposes a fundamental limitation on the lowest BRDF level that can be measured for a surface in a given environment (n, N). No improvement in instrumentation (aside from decreasing ℓ) will improve the BRDF measurement sensitivity of surfaces.

Equation (11) has a singular point at $\eta = \pi/2$. This is due to the mathematical construction of the problem. We arbitrarily choose the orientation of the disk A_d for simplicity to have its normal perpendicular to the optical axis. The radiance from this disk goes to zero at $\eta = \pi/2$. If the orientation of disk A_d were chosen differently, the direction of η for which the radiance would go to zero would be different. This problem is unique to the application of the BRDF to volume sources because the BRDF is truly defined only for surfaces (for which radiance can be defined). Therefore, to obtain an equivalent BRDF for a volume of scatterers when the geometry of the application includes a singularity, it would be best to use the cosine-corrected BRDF, $f' = f\cos\eta$.

The equivalent BRDF in Eq. (11), f, can be expressed as $\ell\beta(\eta_o)/|\cos\eta_o|$, where $\beta(\eta_o)$ is the volume differential scattering coefficient[6] with a dimension of inverse millimeters per steradian; $\beta(\eta_o)$ is defined as the product $N\sigma(\eta_o)$, where $\sigma(\eta_o)$ is the differential scattering cross section for one gas molecule. This expression provides an important link between scattering from volumes and from surfaces.

3. Calculation of Theoretical Equivalent BRDF

The indices of refraction for selected gases are listed in Table 1 in order of descending values[7] for STP conditions at the wavelength of 589 nm. We selected three gases (nitrogen, clean air, and helium) from this list to be used for investigating the influence of Rayleigh scattering on equivalent BRDF measurements.

The theoretical equivalent BRDF values are tabulated in Table 2 according to Eq. (12) for nitrogen, clean air, and helium, and the number density,[8] N, of 2.68×10^{19} molecules/cm^3; we use $\ell = 50$ mm and the wavelengths of 442 and 633 nm (the values used in the experimental system that is discussed in Section 4). These theoretical calculations are based on a simple model. This model assumes that the Rayleigh scattering is caused by individual molecules. One may use this theoretical expression to indicate the effect of several measurement parameters; however, the analysis may not be able to predict exactly the absolute equivalent BRDF values.

Table 1. Index of Refraction for Selected Gases at STP

Gas	n
Freon 22	1.0035
Freon 12	1.0016
Nitrogen	1.000297
Air	1.000293
Argon	1.000281
Oxygen	1.000272
Water (vapor phase)	1.000254
Helium	1.000036

4. Instrumentation

Figure 2 shows a diagram of the low-background reference system (LBRS). All the assumptions that are used to derive Eq. (12) are maintained for the LBRS, i.e., vertically polarized collimated incident light, $\ell \ll r_o$, $n \approx 1$, and $\eta_o = 135°$. The system includes two lasers: helium cadmium at 442 nm and helium neon at 633 nm. The light from each laser is spatially filtered and formed into a collimated beam that has a $1/e^2$ diameter of 4 mm. A dichroic filter selects one of the two beams, which is then directed through a chopper, a baffle, mirror M1, baffle B1, baffle tube P1, and into the LBRS chamber. Baffle B1 is located 75 mm from mirror M1 and 75 mm from baffle tube P1. The sample holder is centrally located within the chamber (0.7 m × 0.75 m × 0.33 m, L × W × H) and can accommodate round samples that have a diameter from 25 to 100 mm. The inside surfaces of the chamber are lined with black-flocked paper (for diffuseness), which was painted over with flat-black paint (for low reflectance). The air inside the chamber can be purged with a gas. Research-grade purity gas (99.9995% pure) is passed through a 0.2-μm filter before entering the chamber. The whole LBRS is contained in a class 10 clean room. An airborne particle counter placed inside the cham-

Table 2. Theoretical Equivalent BRDF Values at Two Wavelengths[a]

BRDF (1/sr)	Wavelength (nm)	
	442	632.8
f_{N_2}	2.24×10^{-7}	5.34×10^{-8}
f_{air}	2.18×10^{-7}	5.22×10^{-8}
f_{He}	3.30×10^{-9}	7.86×10^{-10}

[a] $N = 2.68 \times 10^{19}$ molecules/cm^3, $\ell = 50$ mm.

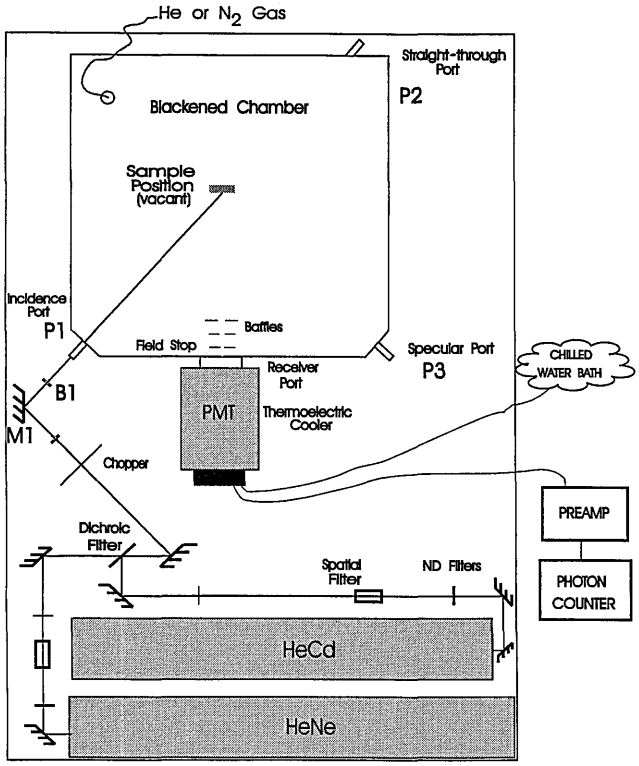

Fig. 2. Layout of the LBRS (not to scale); ND, neutral density.

ber during a purge recorded a cleanliness level that is better than class 10.

The chamber has four oversized light ports: incidence, specular, receiver, and straight-through. The incidence port allows the beam to enter the chamber and strike a sample at its center with a 45° angle of incidence. Baffle tube P1 with an i.d. of 15 mm and that is 75 mm long is mounted on the incidence port. The receiver port admits light through two baffles and one field stop in front of the detector. The specular port is mounted with baffle tube (15 mm i.d. and 75 mm long) P3, which is sealed with a Blue Sky Research Blackhole Laser Beam Trap[9] to capture any light that is specularly reflected from a sample. Baffle tube (23 mm i.d. and 75 mm long) P2 is mounted on the straight-through port. A cornucopia-shaped glass beam trap with a 51-mm-diameter opening is placed ~30 cm away from baffle tube P2 so that the incident beam can exit the chamber when no sample is present.

An oversized volume between baffle tube P2 and trap is enclosed by black rubberized vinyl so that no light can enter. This prevents most of the light that is not absorbed by the trap from reentering the chamber. The baffle tubes and traps are sufficiently oversized to ensure that the fringes of the collimated beam will not be truncated, thereby causing scatter at the edges. The incident beam admitted through P1 is surrounded with a cone of light caused by system scatter, including mirror M1 and the Gaussian beam tail. Some of the scatter cone may enter the photomultiplier tube (PMT) by diffracting from baffle B1 and baffle tubing P1 and scattering off the back chamber wall that is directly in the field of view of the PMT. The specular and receiver ports are also sealed to prevent light from entering the chamber. Although room lights are kept off during measurements, a small amount of light from the laser discharge glow and equipment pilot lights leaks into the chamber through the entrance port. This leakage is mainly the stray light for the system.

We employ photon-counting methods in the detection system to achieve low-level signal measurements. A Hamamatsu[9] PMT Model R943-02 was selected for its good quantum efficiency in the visible and its compatibility with photon-counting techniques. Cooling the selected PMT to −20 °C reduces the dark counts from ~50,000 counts/s (cps) to ~20 cps. The anode current is amplified 25× and is put into the input of the photon counter. Thermal emission from the PMT dynodes and base-amplifier electron noise create a large number of small amplitude pulses. These pulses exhibit less gain than those originating at the photocathode by photon excitation. That is, pulses caused by single photons hitting the photocathode are Poisson distributed about a central pulse-height value that is larger in amplitude than that of the noise pulses. To maximize the ratio of signal pulses to noise pulses in photon counting, one should locate a discriminator at the pulse height that falls between the peaks corresponding to the noise and signal pulses. A pulse-height distribution was obtained for the selected PMT, and the optimum discriminator level was chosen. The PMT receiver system has a dead time of ~10 ns. We applied corrections for dead time to all photon-counting data to compensate for counting losses.[10] The maximum correction required was 2.5% of the counts.

Uncertainties were introduced because some small quantity of noise (and signal) pulses appears with an amplitude larger (and smaller) than the selected discriminator level. There also was a considerable settling time required for the signal counts to stabilize. We separated stray light from the measurement by employing a chopper and the two channels incorporated in the photon counter in the A–B mode.

One field stop and two baffles were placed in front of the PMT (see Fig. 2). The maximum field of view for the receiver system is depicted in Fig. 3 and was set to be 0.0041 sr throughout the entire measure-

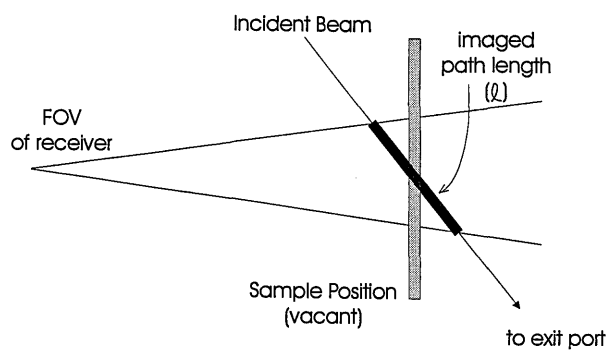

Fig. 3. Field of View (FOV) of the receiver system.

ment so that the path length, ℓ, of the laser beam that is viewed by the receiver is 50 mm. The laser beam bisects the front of the sample holder. When there is no sample present, the angle subtended by $\ell = 50$ at the receiver is ±3°. When there is a sample present, the intecepted laser spot subtends ±0.5° at the receiver. The reflection from the polytetrafluoroethylene (PTFE) sample and the scattering from the gases are both isotopic; the effect of any spatial nonuniformity on the PMT photocathode is negligible. However, because the receiver system does not image the sample onto the PMT photocathode, some parts of the photocathode view all the 50-mm path length and some do not. This poses a potential problem for the system calibration.

The LBRS-equivalent BRDF's were calculated relative to the BRDF of a sintered PTFE sample of known BRDF at 45° angle of incidence and 0° angle of viewing geometry. When measuring the light scattered from the sintered PTFE, we inserted neutral-density filters with a calibrated optical density in front of the lasers to attenuate the signal received to a value below the PMT saturation level. Therefore we determined the equivalent BRDF for the LBRS according to

$$f = (B - B_n) f_R \frac{T}{R - R_n}, \tag{13}$$

where

B is the signal when the chopper is on but no sample is present in the LBRS,

B_n is the stray light detected when the chopper is closed and there is no sample present,

f_R is the BRDF value of the reference sintered PTFE sample,

R is the signal obtained when the reference sintered PTFE sample is present,

R_n is the stray light detected when the chopper is closed and the reference sintered PTFE sample is present, and

T is the transmittance of the neutral-density filters used during the measurement of R.

Ideally, a measurement of the system stray light would involve having the chopper open with no sample in place and no gas present (i.e., a vacuum). The interreflections of the chopped light throughout the chamber would then be taken into account. This type of measurement was impossible to perform because it would have required a vacuum, which was not practical. We greatly minimized interreflections by restricting the field of view, enlarging the entrance and exit ports and their associated baffle tubes, blackening the walls, and using the various beam dumps.

The transmittance value for each of the three two-order neutral-density filters for the two lasers was measured. The combined transmittance of three filters is $T = 3.74 \times 10^{-7}$ for the 442-nm wavelength and $T = 1.85 \times 10^{-6}$ for the 633-nm wavelength, with 2σ uncertainties of approximately 60% and 30%, respectively. These uncertainties are mainly due to random fluctuations in the source and receiver signals and contain a small uncertainty caused by filter replacement or nonuniformity uncertainty. Ignoring the interreflections between these three neutral-density filters causes less than 1% of the combined transmittance values.

5. Experimental Results and Comparison with Theory

We allowed the lasers and receiver system as well as the purge to reach a steady state before any data were recorded. We determined the signal proportional to the incident power by placing a sintered PTFE sample at the sample position and neutral-density filters in the laser beam. The sintered PTFE and neutral-density filters were removed from the sample chamber, and the scatter from the clean air was then measured as a function of time. This ensured that opening the chamber and removing the calibration standard did not stir up particulates in the chamber, and it permitted a sufficient amount of time for the signal to stabilize. The uncertainty is based on 100 measurements made after the signal stabilized. When the measurement was completed, the sintered PTFE was remounted in the chamber and the neutral-density filters were reinserted in the laser beam, and the incident power was rechecked. We repeated this entire procedure to verify the experiment. To verify that gas molecules were limiting the equivalent BRDF, we purged the chamber at 100 kPa with nitrogen (99.9995% pure) and helium (99.9999% pure), and we repeated the experiment by using the procedure stated above.

The stray light entering the system with the laser on, but blocked by the chopper, was recorded at ~700 cps (~2×10^{-13} mW for 633 nm, ~3×10^{-13} mW for 442 nm). We subtracted this stray light from the signal measurements by using the A–B chopping mode of the photon counter. We obtained the uncertainty by adding in quadrature the relative standard uncertainties for each term in Eq. (13):

$$\left(\frac{\Delta f}{f}\right) = \left[\left(\frac{\Delta B}{B - B_N}\right)^2 + \left(\frac{\Delta B_n}{B - B_N}\right)^2 + \left(\frac{\Delta f_R}{f_R}\right)^2 + \left(\frac{\Delta T}{T}\right) + \left(\frac{\Delta R}{R}\right) + \left(\frac{\Delta R_n}{R - R_n}\right)^2\right]^{1/2}. \tag{14}$$

Table 3 contains the equivalent BRDF and the uncer-

Table 3. Measured Equivalent BRDF, f, and Its Uncertainty, Δf, for Three Gases at Two Wavelengths (ℓ = 50 nm)

	Wavelength			
	442 nm		633 nm	
BRDF	f(1/sr)	$\Delta f(2\sigma)$	f(1/sr)	$\Delta f(2\sigma)$
f_{N_2}	6.85×10^{-8}	$\pm 2 \times 10^{-8}$	1.00×10^{-8}	$\pm 0.4 \times 10^{-8}$
f_{air}	7.55×10^{-8}	$\pm 2 \times 10^{-8}$	1.01×10^{-8}	$\pm 0.4 \times 10^{-8}$
f_{He}	1.12×10^{-8}	$\pm 0.3 \times 10^{-8}$	0.15×10^{-8}	$\pm 0.06 \times 10^{-8}$

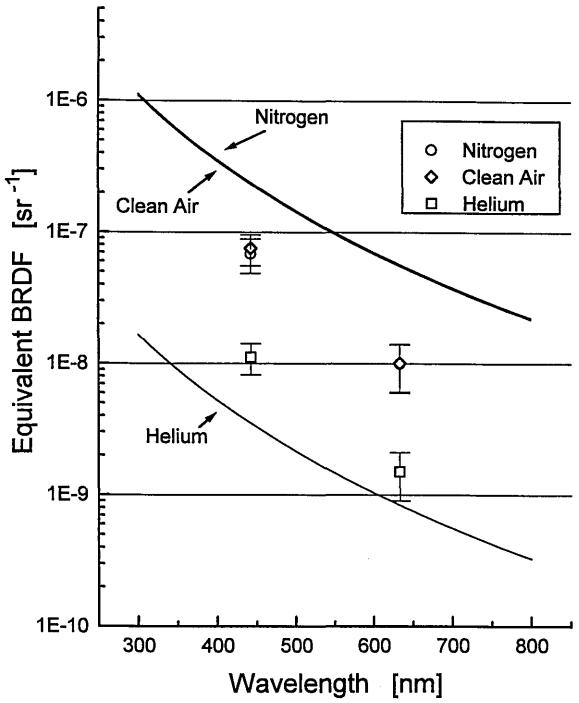

Fig. 4. Plot of theoretical equivalent BRDF as a function of wavelength with experimental data at 442 and 633 nm for nitrogen, air, and helium.

tainties (2σ) for the three gases at the two wavelengths. The theoretical and measured values are shown graphically in Fig. 4, where the experimental equivalent BRDF is plotted versus wavelnegth for nitrogen, clean air, and helium, along with the theoretical prediction for each gas. The measurement uncertainties $\Delta f(2\,\sigma)$ are also shown.

6. Discussion

The experimental uncertainty might be larger than the estimation. This may be one of the reasons that the measured equivalent BRDF's for nitrogen, clean air, and helium are not exactly the same as the theoretical values. The data show that the equivalent BRDF values for nitrogen and clean air are very close. This is expected because the indices of refraction for nitrogen and clean air are nearly the same. The ratio of the measured BRDF value at 422 nm to that at 663 nm for each gas scales with wavelength to the inverse fourth power only when 2σ measurement uncertainty was used. This may have been caused by the presence of a constant noise source that does not scale as inverse wavelength to the fourth power. The ratio of the measured BRDF value for nitrogen or clean air to that of helium is smaller by an order of magnitude at both wavelengths from the theoretical prediction. This could be caused by a source of background noise in the measurement.

7. Conclusions

In general, equivalent BRDF measurements made on BRDF instruments are limited by stray light. This stray light may originate at the optical components used within the system, or it may be caused by interreflections of light from surrounding fixtures. If stray light is minimized within the system, then Rayleigh scattering effects may begin to limit the equivalent BRDF of the system. This study applies to systems in which the stray light does not dominate the equivalent BRDF, and it reveals that BRDF measurements for many common instrument configurations ultimately are limited by atmospheric scattering. This scattering is dependent on the index of refraction of the gas contained within the measurement system, the size of the gas volume viewed, and the wavelength of the light used. The theoretical calculation for the lowest equivalent BRDF level measurement in clean, particle-free air is $\sim 5 \times 10^{-8}$ sr^{-1} (for $\ell = 50$ mm); the experimental value is lower than this value. This may be because of the underestimation of the experimental uncertainty. This equivalent BRDF may be reduced further if the area surrounding the sample and receiver is purged with helium. The size of the field of view of the system permits adjustability of this equivalent BRDF for a given wavelength and gas. The minimum value of the field of view is determined by the extent of the laser beam spot size at the sample (to ensure overviewing), and its maximum is limited by stray-light considerations. Photon counting was used for these experiments because of its high sensitivity; however, other more stable techniques may be employed to achieve low-level BRDF measurements if they have comparable sensitivity.

Appendix A. Derivation of Irradiance Caused by Rayleigh Scattering of Vertically Polarized Incident Light

Here we derive the expression for the irradiance caused by Rayleigh scattering as a function of physical parameters and geometrical arrangement. The Stokes parameters[5] for the incident light can be expressed in terms of a, x, and ψ (see Fig. 5):

$$
\begin{aligned}
E_i &= \frac{c}{8\pi}\langle a^2\rangle, \\
Q_i &= E_i \cos 2\chi \cos 2\psi, \\
U_i &= E_i \cos 2\chi \sin 2\psi, \\
V_i &= E_i \sin 2\chi, \qquad \text{(A1)}
\end{aligned}
$$

where

E_i is the incident irradiance,

Q_i is the horizontal polarization preference component,

U_i is the $+45°$, $+135°$ polarization preference component,

V_i is the right circular polarization preference component,

a is the amplitude of the electric field,

c is the speed of light, and

χ and ψ are elliptical expressions of phase angles of the electric field as illustrated in Fig. 5 ($-\pi/4 \le \chi \le \pi/4$, $\quad 0 \le \psi \le \pi$).

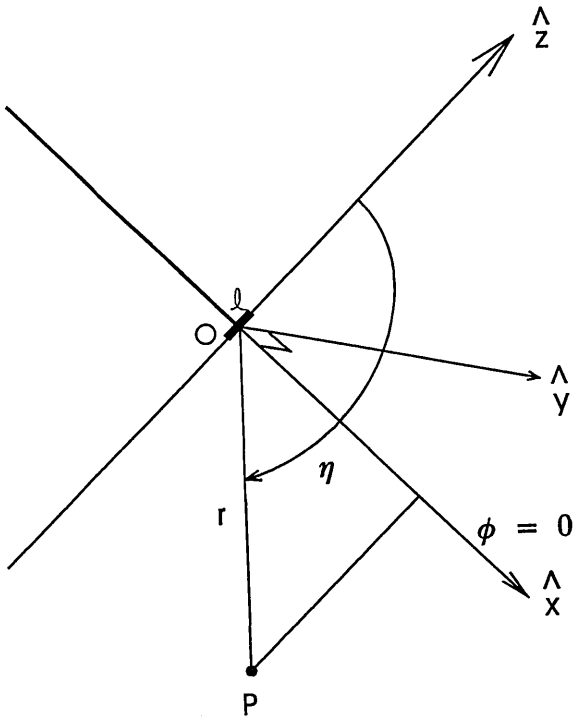

Fig. 5. Ellipse expression of electric field parameters a, χ, ψ.

According to Stone,[5] the Stokes parameters of the scattered light at point p can be expressed as

$$\begin{aligned}
E_p &= \tfrac{1}{2}(|\tau_{\eta x}|^2 + |\tau_{\phi x}|^2)(E_i + Q_i) \\
&\quad + \tfrac{1}{2}(|\tau_{\eta y}|^2 + |\tau_{\phi y}|^2)(E_i - Q_i) \\
&\quad + R_e(\tau_{\eta x}\tau_{\eta y}^* + \tau_{\phi x}\tau_{\phi y}^*)(U_i + iV_i), \\
Q_p &= \tfrac{1}{2}(|\tau_{\eta x}|^2 - |\tau_{\phi x}|^2)(E_i + Q_i) \\
&\quad + \tfrac{1}{2}(|\tau_{\eta y}|^2 - |\tau_{\phi y}|^2)(E_i - Q_i) \\
&\quad + R_e(\tau_{\eta x}\tau_{\eta y}^* - \tau_{\phi x}\tau_{\phi y}^*)(U_i + iV_i), \\
U_p + iV_p &= \tau_{\eta x}\tau_{\phi x}^*(E_i + Q_i) + \tau_{\eta y}\tau_{\phi y}^*(E_i - Q_i) \\
&\quad + \tau_{\eta x}\tau_{\phi x}^*(U_i + iV_i) + \tau_{\eta y}\tau_{\phi x}^*(U_i - iV_i).
\end{aligned} \tag{A2}$$

For Rayleigh scattering,

$$\begin{aligned}
\tau_{\eta x} &= \frac{k^2\alpha}{r}\cos\eta\cos\phi\exp(ikr), \\
\tau_{\eta y} &= \frac{k^2\alpha}{r}\cos\eta\sin\phi\exp(ikr), \\
\tau_{\phi x} &= -\frac{k^2\alpha}{r}\sin\phi\exp(ikr), \\
\tau_{\phi y} &= \frac{k^2\alpha}{r}\cos\phi\exp(ikr),
\end{aligned} \tag{A3}$$

where

τ's are transfer functions based on the geometry of the optical system,

k is the wave number, i.e., $2\pi/\lambda$,

α is the polarizability of dimension [m^3], and

r is the distance of point p to the center of the geometric coordinate system.

The relations between x, y, η, and ϕ are shown in Fig. 6.

For vertically polarized incident light,

$$\chi = \pi/2, \qquad \psi = 0.$$

The Stokes parameters of Eq. (A1) can be simplified to

$$[E_i, Q_i, U_i, V_i] = [E_i, -E_i, 0, 0], \tag{A4}$$

where

$$E_i = \frac{c}{8\pi}\langle a^2\rangle.$$

Inserting Eq. (A4) into Eqs. (A2) and (A3), we have

$$\begin{aligned}
E_p &= \frac{k^4\alpha^2}{r^2}(\cos^2\eta\sin^2\phi + \cos^2\phi)E_i, \\
Q_p &= \frac{k^4\alpha^2}{r^2}(\cos^2\eta\sin^2\phi - \cos^2\phi)E_i, \\
U_p &= 2\frac{k^4\alpha^2}{r^2}(\cos\eta\sin\phi\cos\phi)E_i, \\
V_p &= 0,
\end{aligned} \tag{A5}$$

For point p on the x–z plane, $\phi = 0$. The Stokes parameters at point p in the x–z plane, with vertically

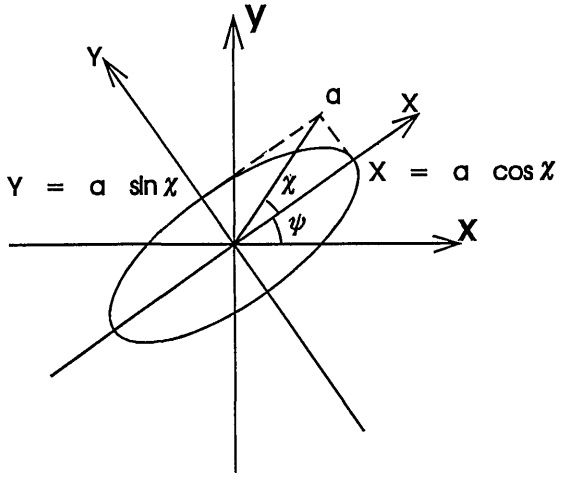

Fig. 6. Geometric coordinates for scattering.

polarized light caused by Rayleigh scattering of one gas molecule, can be expressed as

$$E_p = \frac{k^4\alpha^2}{r^2} E_i,$$
$$Q_p = E_p,$$
$$U_p = 0,$$
$$V_p = 0. \tag{A6}$$

We acknowledge W. Kemp of the Phillips Laboratory for discussions about minimum equivalent BRDF determination. We also thank J. Proctor and R. Deb of the National Institute of Standards and Technology for their assistance in carrying out the measurements.

References and Notes

1. F. E. Nicodemus, J. C. Richmond, J. J. Hsia, I. W. Ginsberg, and T. Limperis, "Geometrical considerations and nomenclature for reflectance," Natl. Bur. Stand. (U.S.) Monogr. **160,** 1–8.
2. "Standard practice for angle resolved optical scatter measurements on specular or diffuse surfaces," Am. Soc. Test. Mater., standard designation E 1392-90 (1991).
3. J. C. Stover, K. A. Klicker, D. R. Cheever, and F. M. Cady, "Reduction of instrument signature in near angle measurements," in *Metrology: Figure and Finish,* B. E. Truax, ed., Proc. Soc. Photo-Opt. Instrum. Eng. **749,** 46–53 (1987).
4. K. A. Klicker, J. C. Stover, D. R. Cheever, and F. M. Cady, "Practical reduction of instrument signature in near specular light scatter measurements," in *Current Developments in Optical Engineering II,* R. E. Fisher and W. J. Smith, eds., Proc. Soc. Photo-Opt. Instrum. Eng. **818,** 26–33 (1987).
5. J. M. Stone, *Radiation and Optics* (McGraw-Hill, New York, 1953), pp. 313–322, 340–343.
6. E. J. McCartney, *Optics of the Atmosphere—Scattering by Molecules and Particles* (Wiley, New York, 1976), p. 192.
7. *Handbook of Chemistry and Physics,* 70th ed. (CRC, Boca Raton, Fla., 1989–1990), p. E386.
8. The number of gas molecules per unit volume, N, is calculated from Avogadro's law, which states that under the same conditions of pressure and temperature, equal volumes of all gases contain equal numbers of molecules, namely, 6.023×10^{23} molecules/mol. The volume occupied by 1 mol of an ideal gas at STP (0 °C, 1.01×10^5 Pa) is 22.414 L. Thus the number of gas molecules per unit volume is given by

$$N = \frac{(6.023 - 10^{23}\ \text{molecules/mol})}{(22.414\ \text{L/mol} - 1000\ \text{cm}^3/\text{L})}$$
$$= 2.68 \times 10^{19}\ \frac{\text{molecules}}{\text{cm}^3}.$$

9. Certain commercial equipment or materials are identified in this paper only to specify the experimental procedure adequately; they are not necessarily the best available for the purpose. Such identification is not a recommendation or endorsement by the National Institute of Standards and Technology.
10. E. Bleuler and G. J. Goldsmith, *Experimental Nucleonics,* (Holt, Rinehart & Winston, New York, 1960), p. 59.